


Temperature dependence of dynamic dipole formation in PbTe

Kristoffer A. U. Holm¹, Nikolaj Roth, Christian M. Zeuthen, Kasper Tolborg, Anders A. Feidenhans'l¹, and Bo B. Iversen^{*}
Center for Materials Crystallography, Department of Chemistry and iNANO, Aarhus University, DK-8000 Aarhus C, Denmark

 (Received 9 May 2020; accepted 26 June 2020; published 29 July 2020)

PbTe-based thermoelectric materials remain of great interest due to their peculiar dynamic behavior and high thermoelectric performance. The true structure of pristine PbTe has been widely discussed, since the average rocksalt structure does not adequately account for the low lattice thermal conductivity. Single crystals of PbTe exhibit large amounts of x-ray diffuse scattering, which along with additional experimental observations has led to a series of structural models containing different types of disorder. Recently, analysis of the x-ray diffuse scattering from single-crystal PbTe confirmed the formation of local dynamic dipoles proposed earlier based on inelastic neutron scattering (INS) and one-dimensional pair distribution function (PDF) experiments. Here, we study the single-crystal diffuse x-ray scattering over a wider temperature range from 30 to 622 K in order to investigate the temperature dependence of the dynamic dipole formation. We observe that the longitudinal displacement correlations along the $\langle 100 \rangle$ directions form pairwise plateaus which results in a steplike decay of the correlations with increasing interatomic distance. This is consistent with previous observations from single-crystal diffuse scattering experiments on PbTe where the same steplike trend for the correlations was observed. However, upon lowering the temperature we observe a larger relative antiphase displacement contribution to the correlations proposed to originate from the softening of the transverse optical (TO) branch. As the local dipole formation depends on the absolute amplitude of antiphase displacements, and not the relative antiphase contribution to atomic displacements, it is found that the local dipole formation increases upon heating consistent with previous INS and PDF studies. The underlying mechanism responsible for the softening of the TO branch, and thereby the formation of dynamic dipoles, is investigated by comparison to the isostructural KCl system. The different dynamics in KCl and PbTe can be explained from the different bonding mechanism, where the metavalent bonding and ability to dynamically express a stereochemically active lone pair in PbTe gives rise to long-range interactions and TO phonon softening.

DOI: [10.1103/PhysRevB.102.024112](https://doi.org/10.1103/PhysRevB.102.024112)

I. INTRODUCTION

Understanding structure-property relations lies at the very foundation of functional materials development. When it comes to crystalline materials, these relations are often established by comparing the average crystal structure determined by x-ray-diffraction techniques to various physical properties of interest. Such conventional x-ray-diffraction techniques rely on the assumption of a perfectly periodic, ordered structure. However, sticking with the IUCr definition of a crystalline solid [1], we note that this includes statically or dynamically disordered materials. For these crystalline materials, the spatial and temporal average structure, which gives rise to the sharp Bragg reflections, deviates from the real structure. The disorder in these materials gives rise to diffuse scattering not limited to the nodes of the reciprocal lattice. Examples of disorder breaking the translational symmetry of the crystal lattice include the structural disorder caused by vacancy ordering in systems with a defect stoichiometry [2–6], structures with disordered stacking of ordered layers [7–11], and dynamically disordered structures [12–15].

For such disordered crystals, it is of interest to understand in greater detail the local structure of the material as this

will affect the physical properties. In order to achieve this, one may exploit the information available from the reciprocal space distribution and intensity of the diffuse scattering. One practical approach to this is to use the three-dimensional difference pair distribution function (3D- Δ PDF) to investigate local correlations in direct space [16]. The x-ray 3D- Δ PDF is the temporal average of the autocorrelation of the difference electron density ($\delta\rho = \rho - \rho_{\text{avg}}$ where ρ_{avg} is the periodic, average density and ρ is the actual density), and it can be obtained experimentally as the inverse Fourier transform of the x-ray diffuse scattering intensity:

$$3\text{D-}\Delta\text{PDF} = \mathcal{F}^{-1}(I_{\text{diffuse}}) = \langle \delta\rho \otimes \delta\rho \rangle.$$

Here \mathcal{F} denotes the Fourier transform and \otimes denotes the cross-correlation operator. The 3D- Δ PDF may be interpreted as the difference between a generalized Patterson function of the real structure and the Patterson function of the average, periodic structure. Thus, the 3D- Δ PDF will have positive features for vectors separating more electron density in the real structure compared to the average structure and negative features have an analogous interpretation. This makes the 3D- Δ PDF an extremely useful tool when it comes to solving the local structure of statically disordered materials [7,17,18].

Disorder is often favorable in thermoelectric materials as the lattice thermal conductivity may be lowered by phonon-defect scattering [19]. This makes disorder, an important

^{*}Corresponding author: bo@chem.au.dk

variable in the optimization of thermoelectric materials as the thermoelectric figure of merit is inversely proportional to the total thermal conductivity. Such important relations between local structure and technological applications warrant the use of methods such as the 3D- Δ PDF method or more conventional one-dimensional pair distribution function (1D-PDF) methods [20].

Recently, the structure of PbTe has been scrutinized carefully due to its technological relevance. In the field of thermoelectrics, PbTe is an important base material for the design of complex thermoelectric materials due to properties such as a low lattice thermal conductivity [21] and a favorable electronic structure that may be optimized by doping with various elements [22]. Several studies have investigated the origin of the low lattice thermal conductivity. Inelastic neutron-scattering experiments have revealed a large degree of anharmonicity in PbTe [23,24], which has been found by first-principles anharmonic lattice dynamics to lead to increased scattering between longitudinal acoustic and transverse optical phonons, which along with the low group velocity of the transverse acoustic modes leads to a limited lattice thermal conductivity [25]. Recently, it has been shown that an even lower thermal conductivity may be obtained by inducing line defects in the form of dislocations by high-energy ball milling. The effect of such treatment was shown to be an effective lowering of the speed of sound in the material directly leading to a lowered thermal conductivity [26].

The local structure of PbTe has also been investigated in order to uncover any disorder contributions to the lowering of the lattice thermal conductivity. The neutron 1D-PDF of PbTe has been found to display highly non-Gaussian nearest-neighbor peaks which appear upon heating and show an anomalous broadening with temperature [27]. This phenomenon, which was attributed to the formation of local dipoles, was coined *emphanis* [27–29]. It was argued that the asymmetry of the nearest-neighbor peak was consistent with a displacement of Pb from its center position in the Te coordinating octahedron of up to $\delta_{500\text{ K}} = 0.24 \text{ \AA}$ [27]. While it was not possible to ascertain whether the displacement was of static or dynamic nature from the PDF data due to the inherent temporal averaging, inelastic neutron-scattering experiments indicated a dynamic origin [28]. However, the possibility of static off-centering has been considered in several studies. Analysis of the Pb probability density extracted by Gram-Charlier analysis of powder x-ray-diffraction (PXRD) data showed no clear indications of Pb off-centering within uncertainties estimated by Monte Carlo simulations [30]. Further analysis of the electron weighted nuclear density distribution (eNDD) extracted using the nuclear-weighted x-ray maximum entropy method [31] on PXRD data collected at 100 K was also unable to resolve whether the Pb atoms were in fact displaced from their center positions [30]. Recently, additional uncertainties were sparked as to the accuracy of average structures determined by powder x-ray-diffraction based methods for the lead chalcogenides [32]. Systematic trends in peak broadening with Miller indices were attributed to a varying diffuse scattering contribution to different Bragg peaks as can be understood by the fact that the strong diffuse scattering near the Bragg peaks assumed anisotropic shapes dependent on the scattering vector. These shapes can be attributed to the

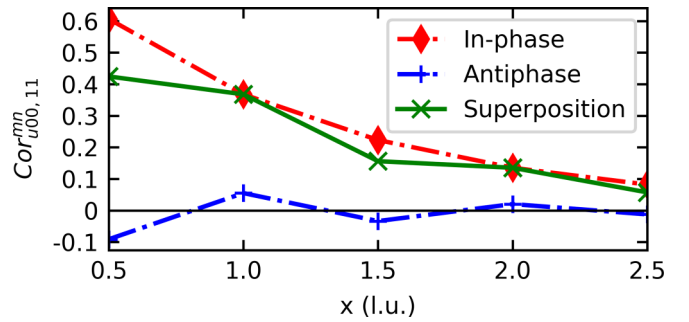


FIG. 1. Illustration showing the effect of a superposition (green x 's) of in-phase displacements (red diamonds) and antiphase displacements (blue crosses) on the longitudinal displacement correlations along $\langle 100 \rangle$. The figure is inspired by [12].

dependence of the thermal diffuse scattering (TDS) intensity on the polarization of the contributing phonons [13]. When the orientational average inherent to powder-diffraction methods is taken, the varying shapes of the diffuse scattering will contribute differently to the width of Bragg peaks depending on the Miller indices, thus resulting in the trends observed by Zeuthen *et al.* [32]. It is speculated that such contributions to the structure factors given as input to maximum entropy method calculations could bias the results adding additional uncertainties to conclusions about static lead off-centering [33].

The dynamic origin of the local dipole formation proposed by Jensen *et al.* [28] was further investigated by Sangiorgio *et al.* [12], who analyzed the system using *ab initio* molecular dynamics, refinement of atomic displacement correlations against x-ray single-crystal diffuse scattering, and analysis of the corresponding 3D- Δ PDFs. The results were rationalized in terms of the soft transverse optical (TO) modes near the Γ point. It was observed experimentally that the longitudinal displacement correlations along $\langle 100 \rangle$ formed pairwise plateaus resulting in a steplike decay along these directions. This steplike trend was rationalized in terms of a superposition of in-phase displacements, which give a purely positive contribution to the displacement correlations, and antiphase displacements, which give rise to an alternating sign contribution along $\langle 100 \rangle$; see Fig. 1. Having a relatively higher weight of the in-phase contributions compared to the antiphase contributions results in the steplike trend in correlations observed experimentally. It was argued that while in-phase displacements could be brought about by the acoustic phonons near the zone center, which are highly occupied at any temperature, the antiphase displacements could result from the TO soft modes near Γ .

The contribution from the antiphase displacements of atoms leads to a Pb-Te “dimerization.” This results in the formation of dynamic local dipoles without any static Pb off-centering. This interpretation is consistent with the origin of the local dipole formation being the near zone center TO modes as proposed by Jensen *et al.* [28]. However, while no significant temperature dependence was observed by Sangiorgio *et al.* [12] a large temperature dependence was observed in previous studies [27,28]. Some temperature dependence should be expected based on the dynamic origin of

the phenomenon and on the phonon-energy and temperature dependence of the phonon Bose-Einstein populations.

The aim of this study is therefore to analyze the temperature dependence of the diffuse scattering and direct-space displacement correlations over a wider temperature range (from 30 to 622 K) as such an investigation will be able to further clarify the origin of the diffuse scattering and relate it to the proposed dynamic origin [12,28]. By comparison to a well-known rocksalt structure system, potassium chloride, in which no soft TO mode is expressed [34], the interpretation is tested further and differences between the two systems are interpreted in terms of differences in chemical bonding in the two systems.

The analysis and interpretation of the extracted displacement parameters is divided into two. First, the relative contribution of antiphase displacements to the longitudinal displacement correlations along (100) are interpreted in terms of the TO branch softening near the Brillouin-zone center. Then, the extent of local dipole formation is analyzed through the absolute contribution of antiphase displacements along (100).

II. METHODS

A. Synthesis of PbTe and KCl single crystals

PbTe single crystals were synthesized through sublimation and subsequent growth from a pure PbTe charge. The charge was synthesized by melting the pure elements in a fused silica ampoule at 1000 °C. The transport was done at 1000 °C with a continuous flow of N₂ gas over the ampoule to cool parts of the ampoule to a suitable growth temperature. The transport was done for 5 h to ensure small single crystals. KCl was crystallized from a saturated aqueous solution.

B. Average structure experiments

Single-crystal Bragg diffraction data were collected at BL02B1, Spring8, Japan. Data sets were collected at 20, 100, 200, and 300 K using a cylindrical image plate detector and a wavelength of 0.24896 Å. Data were collected on an approximately 100×100×100 μm³ PbTe crystal (crystal A) as 60° ω scans with a 11 s exposure time and a Δω of 10.5°. The data were collected with a 400 μm Ni beam attenuator.

Structural data sets at other temperatures were collected using a Pilatus 1M CdTe photon counting detector and a wavelength of 0.24797 Å. Data were collected on an approximately 80×80×80 μm³ PbTe crystal (crystal B) as 180° ω scans with a 0.2 s exposure time and a Δω of 0.2°. Four detector positions with a 2θ of 0, −10, −20, and −30° respectively were used to increase resolution and redundancy. The data were collected with a 350 μm Ta beam attenuator. Information on the average structure data reduction and solution is given in the Supplemental Material [35] (see, also, Refs. [33,36–45]).

C. Diffuse scattering experiments

Single-crystal diffuse scattering data were measured at BL02B1, Spring8, Japan using wavelengths of 0.246800 Å and 0.24797 Å for crystal A and B respectively. All data sets were collected using a Pilatus 1M CdTe photon counting detector.

Data sets for crystal A were measured from 30 to 100 K in steps of 10 K and from 100 to 300 K in steps of 50 K. At each temperature point data were collected as 180° ω scans with a Δω of 0.2° and an exposure time of 0.5 s. Data were collected with detector positions of 0, −10, −20, and −30° in 2θ.

Data sets for crystal B were measured at the same beam-line using the high-temperature setup. The temperature was calibrated using a thermocouple centered in the goniometer. Data were collected with the same strategy as for crystal A except for a longer exposure time of 1 s per frame.

Diffuse scattering data were also measured on a KCl single crystal of an approximate size of 100×100×100 μm³ using the same strategy as for crystal A and a wavelength of 0.24800 Å.

Air scattering was measured for crystal B (200 frames at each 2θ position) and the KCl crystal (90 frames at each 2θ position). The air scattering was collected by removing the crystal from the beam and measuring data using the same exposure times. For subtraction of air scattering for crystal A the KCl air scattering data is used with a refined scale factor as elaborated in the Supplemental Material [35] (see, also, Refs. [16,46]).

The primary data reduction procedure for diffuse scattering is summarized in the Supplemental Material [35] (see, also, Refs. [12,45,47]).

D. Modeling of diffuse scattering

The YELL code [46] is used for refining the atomic displacement correlations against properly corrected single-crystal x-ray diffuse scattering. In the kinematic and harmonic approximations as well as upon neglecting anomalous scattering and bonding effects the following expression can be derived for the diffuse scattering intensity in the case of purely displacive disorder [16,46]:

$$I_{\text{diff}} = \sum_{\mathbf{R}_{uvw}}^{\text{cryst}} \sum_{mn}^{\text{cell}} \left\{ \exp(-\mathbf{h}^T \beta_{uvw}^{mn} \mathbf{h}) - \exp[-\mathbf{h}^T (\beta_{av}^m + \beta_{av}^n) \mathbf{h}] \right\} \cdot f_m(\mathbf{h}) f_n(\mathbf{h}) \cos[2\pi \mathbf{h}^T (\mathbf{R}_{uvw} + \mathbf{r}_{mn})].$$

The sums run over all atomic pairs in the unit cell each separated by \mathbf{r}_{mn} and all distinct lattice vectors, \mathbf{R}_{uvw} . Points in reciprocal space are denoted by \mathbf{h} , and β_{av}^m and f_m are the average atomic displacement parameters (ADPs) and atomic scattering factors of atom m , respectively. The matrix β_{uvw}^{mn} is the joint displacement matrix of atoms m and n separated by the interatomic vector $\mathbf{R}_{uvw} + \mathbf{r}_{mn}$. The elements of this matrix are directly related to the displacement correlations of the two atoms as the ADP-normalized displacement correlations are defined as

$$\text{Cor}_{uvw,ij}^{mn} = \frac{\langle u_i^m u_j^n \rangle_{uvw}}{\sqrt{\beta_{m,ii}^{av} \beta_{n,jj}^{av}}},$$

where u_i^n is the i th component of the instantaneous displacement of the n th atom given in fractional coordinates. $\langle \dots \rangle_{uvw}$ denotes the temporal and spatial average for all pairs mn separated by the same lattice vectors of indices uvw . The

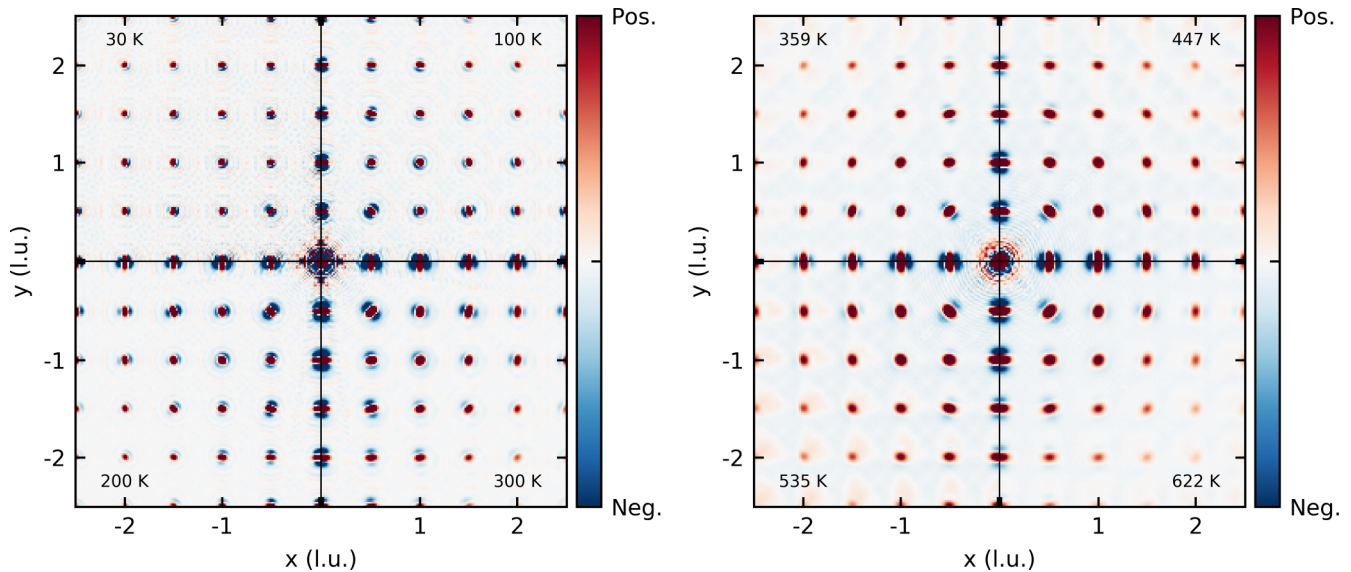


FIG. 2. Representative 3D- Δ PDFs in the $z = 0$ plane at various temperatures (each quadrant in the subfigures corresponds to one temperature). The negative-positive-negative features along the interatomic vectors correspond to positive longitudinal displacement correlations. When one atom displaces in one direction neighboring (and further away) atoms tend to displace in the same direction. The data are displayed on an arbitrary scale.

elements of the joint displacement matrix are given by

$$\beta_{uvw,ij}^{mn} = \langle (u_i^n - u_i^m) (u_j^n - u_j^m) \rangle_{uvw}.$$

Thus, the diffuse scattering resulting from displacement correlations, such as those originating from dynamical disorder, is determined completely by the average structure parameters and the ADP-normalized displacement correlations for all atomic pairs. Thus, the latter (given the knowledge of the average structure) is directly available from the diffuse scattering. Further details on the modeling are given in the Supplemental Material [35] (see, also, Refs. [12,46,48]).

III. RESULTS AND DISCUSSION

A. 3D- Δ PDF

In Fig. 2 representative 3D- Δ PDFs are shown for various temperatures in the $z = 0$ plane (3D- Δ PDFs for the remaining temperatures are available in the Supplemental Material [35]). The positive intensity surrounded by negative intensity at the origin (i.e., an interatomic vector of zero length) corresponds to the atomic motion of a single atom always being completely correlated with itself. Considering the $\langle 100 \rangle$ directions strong negative-positive-negative features are observed. These are a clear sign of overall positive displacement correlations. In the average structure, atoms are assumed to vibrate independently of one another. This will in general lead to a broad distribution of interatomic vectors observed in the Patterson function as a broad, positive peak. In the real structure, atoms often tend to vibrate in phase as a result of having the low-energy, zone-center acoustic-phonon modes occupied to the largest extent. This corresponds to positive displacement correlations. This results in the temporally averaged distribution of interatomic vectors being narrower than in the uncorrelated case. This causes the generalized Patterson function to be narrower than the Patterson function of the average structure. Thus, the

3D- Δ PDF, being the difference between these functions, will display features showing a characteristic negative-positive-negative signature as observed here.

It should be noted that positive displacement correlations are to be expected for many inorganic crystalline solids, even though some may have soft optical-phonon modes near Γ with displacements corresponding to antiphase displacement of atoms. This can be rationalized by the acoustic modes dispersing towards zero energy at the zone center while the optical-mode energies remain finite. According to statistical mechanics these modes are therefore expected to have relatively lower populations. As can be observed from Fig. 2 the positive correlations are especially strong along the $\langle 100 \rangle$ directions. This is consistent with an analysis of the interatomic force constants (IFCs) which shows the interactions to be very strong in these directions [49].

The interactions along $\langle 100 \rangle$ can be analyzed further by considering line plots in the 3D- Δ PDF where the intensity along these directions is plotted. Such line plots are shown for selected temperatures in Fig. 3(a). The line plots for crystal B have been scaled such that the maxima of the peak at $x = 0.5$ for the data measured at 297 K coincides with the corresponding peak for the data measured on crystal A at 300 K. According to the previous discussion on the effect of positive displacement correlations on the 3D- Δ PDF, the amplitude of the positive part of the feature can be loosely interpreted as the magnitude of the positive covariance weighted by the product of the electron densities of the atoms in the atomic pair. As may be expected we observe a decrease in the displacement covariance with increasing length of interatomic vector in Fig. 3(a). It is also apparent that the amplitudes of the features in the 3D- Δ PDF increase with increasing temperature due to the larger amplitudes of the correlated atomic motion. While the electron density weighting of the peaks will favor a steplike trend in the peak amplitudes along $\langle 100 \rangle$ we also

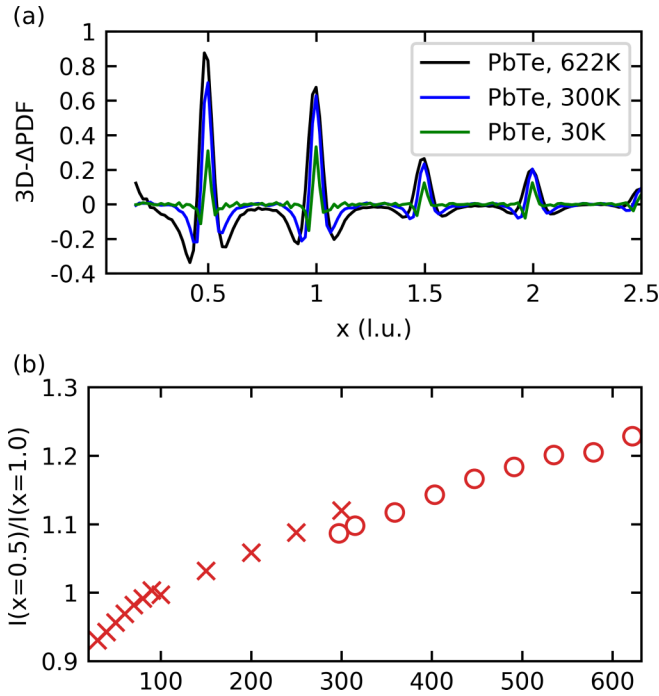


FIG. 3. (a) Line plots of the 3D- Δ PDF intensity along $\langle 100 \rangle$ for three different temperatures in PbTe. (b) Ratios between the peak maximum for the nearest neighbor and next-nearest neighbor along $\langle 100 \rangle$ as a function of temperature. Circles correspond to data on crystal B while x's correspond to data on crystal A.

observe that the steplike trend becomes more pronounced at lower temperatures. This suggests that apart from the electron density weighting there is also a temperature-dependent contribution to the steplike trend from the displacement correlations. In order to qualitatively investigate the temperature dependence of this contribution we plot the ratio between the amplitude of the nearest- and next-nearest-neighbor peak along $\langle 100 \rangle$ as a function of temperature in Fig. 3(b). A smaller ratio corresponds to a more pronounced steplike trend corresponding to a larger relative antiphase contribution to the displacement correlations. It is important to note that this cannot be directly translated into a larger degree of local dipole formation, as this will also depend on the amplitude of the atomic displacements. As can be seen from Fig. 3(b) a decrease in this ratio is observed with decreasing temperature signifying a relatively larger antiphase displacement contribution to the correlations at lower temperatures. In the study by Sangiorgio *et al.* [12] it was concluded that no significant temperature dependence could be observed for the steplike trend in correlations along $\langle 100 \rangle$ which occurs to be inconsistent with the qualitative temperature dependence observed here. In order to analyze this in greater detail numerical values of atomic displacement correlations are needed. These are obtained by refinement against diffuse scattering data.

Figure 4 shows examples of the experimental and modelled diffuse scattering from PbTe at several different temperatures in the $L = 0$ plane of reciprocal space. The lower half of each subfigure shows the residuals from the refinement in

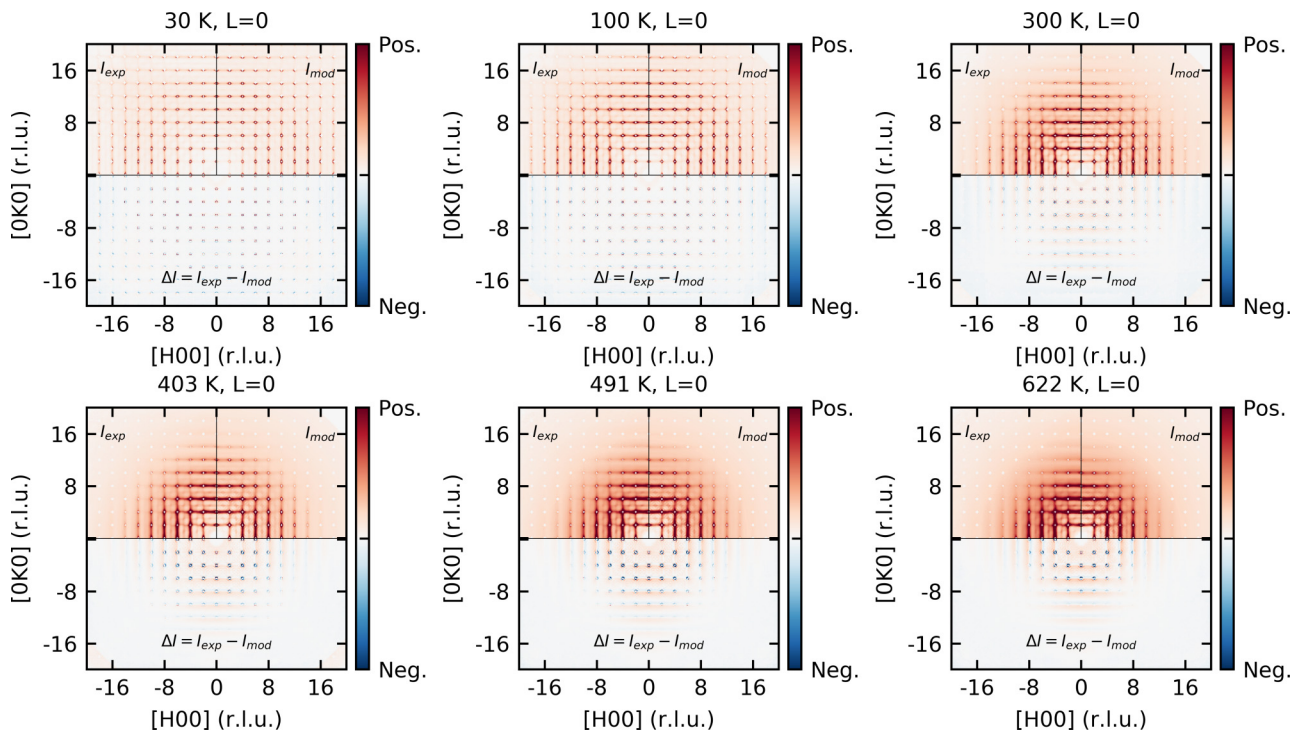


FIG. 4. Examples of experimental and modelled diffuse scattering in the $L = 0$ plane of reciprocal space (upper left and right quadrant of each subfigure respectively) and residuals to the modelled intensity in the same plane (lower half of each subfigure). The data are displayed on an arbitrary scale. Similar figures for more temperatures and other planes are shown in the Supplemental Material [35].

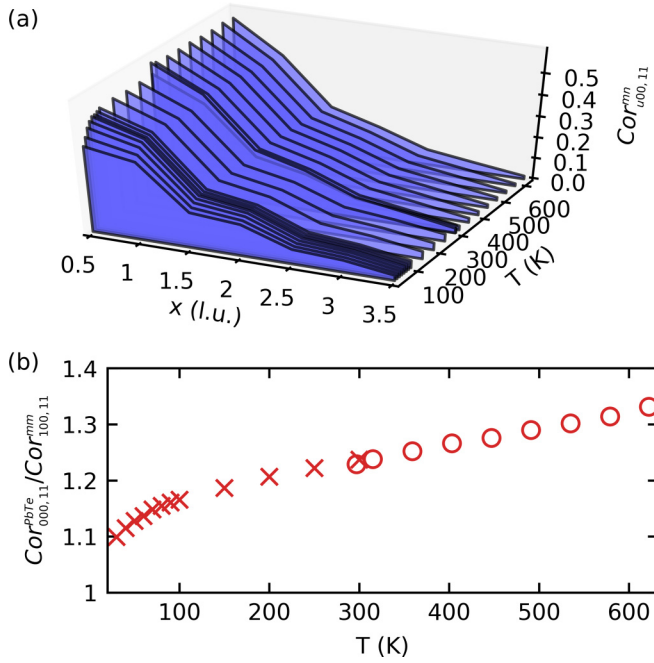


FIG. 5. (a) Displacement correlations along $\langle 100 \rangle$. $Cor_{u00,11}^{mm}$ denotes the longitudinal displacement correlation between the m th and n th atom in unit cells separated by the lattice vector $\langle u00 \rangle$. (b) Ratios of the nearest-neighbor and next-nearest-neighbor displacement correlations along $\langle 100 \rangle$ as a function of temperature. Circles correspond to data on crystal B while x 's correspond to data on crystal A.

the same plane. Reasonable agreement is observed between the experimental and modelled diffuse scattering signal by visual inspection. R_w values of the least-squares fits are summarized in the Supplemental Material [35] and lie in the range of 0.19–0.54. The best fits are obtained in the intermediate temperature range of 100–300 K for crystal A where R_w values similar to previous studies are obtained [12]. The variations in fit qualities and R_w values obtained here can be rationalized by the following considerations. At low temperatures, the diffuse scattering intensities are generally low due to the dynamic origin of the scattering. Thus, the I/σ decreases to a level which makes modeling difficult leading to an increased value of R_w . Crystal B, used for high-temperature measurements, was observed to be more mosaic than crystal A, which makes it more difficult to obtain a high quality fit. Furthermore, PbTe has been shown to exhibit a large degree of anharmonicity [23,24,33] and thus the harmonic model imposed on the data in this study is expected to produce fits of lower quality at high temperatures. The displacement correlations extracted from the diffuse scattering data enables further analysis. In the following section we investigate the relative contribution of antiphase displacements to the atomic displacement correlations. The temperature dependence of this contribution is related to the softening of the TO branch at the Brillouin-zone center.

B. Zone center soft TO mode

In Fig. 5(a) displacement correlations along $\langle 100 \rangle$ extracted from the model are plotted for different tempera-

tures. As can be seen from Fig. 5(a), a pronounced steplike trend is observed at low temperatures, while it becomes less pronounced at elevated temperatures, consistent with what was observed directly from the 3D- Δ PDFs. We want to investigate the temperature dependence of the steplike trend, and therefore a measure for this is needed. This is obtained by taking the ratio of the nearest- and next-nearest-neighbor displacement correlations. A value approaching 1 corresponds to a significant steplike trend in the correlations, while larger values correspond to a less pronounced steplike trend. As observed from Fig. 5(b) the steplike trend becomes stronger at lower temperatures. However, the plot of ratios versus temperature is fairly flat in the region from 100 to 300 K which could explain why no clear temperature dependence was observed over the temperature range studied in [12].

The observed trend with temperature is still consistent with the interpretation made by Sangiorgio *et al.* [12] with slight modifications. As explained before, the significant population of optical-phonon modes is made possible by the soft TO mode at Γ . This results in an alternating sign contribution to the displacement correlations along $\langle 100 \rangle$. Taking into account the purely positive contribution resulting from the populated acoustic modes near the zone center, the resulting displacement correlations follow a steplike trend along $\langle 100 \rangle$. At low temperatures the TO mode at Γ becomes very soft [23,24,28], which mitigates the population decrease resulting from the lower temperature. If the acoustic-phonon dispersions are considered temperature independent, this would result in the steplike trend becoming more pronounced at low temperatures, which is what is observed here. Upon heating we observe a lower relative antiphase displacement contribution to the correlations in Fig. 5, consistent with a hardening of the TO branch. However, the displacement correlations themselves do not accurately reflect the extent of local dipole formation, as (i) the in-phase displacements tend to conserve interatomic vectors, and (ii) the extent of formation of dynamic dipoles also depends on the amplitude of atomic vibrations. Thus, a measure of the dynamic dipole formation which takes these considerations into account is needed. This is explored in the following section.

C. Local dipole formation

In order to define a measure of the dynamic dipole formation, resulting from the absolute contribution of antiphase displacements of atoms, we consider the elements of the joint displacement matrix defined in Sec. II C. The elements of β_{uvw}^{mn} corresponding to longitudinal displacements along $\langle 100 \rangle$ give the mean-square deviation of interatomic distances: $\beta_{u00,11}^{mn} = \langle (u_1^n - u_1^m)^2 \rangle$ where u_1^n is the displacement of atom n along $\langle 100 \rangle$. For large distances, where displacements are uncorrelated, they tend to the sum of the mean-square displacements, i.e., the ADPs (see the Supplemental Material [35] for more details). On the other hand, the atomic displacements are correlated on a local scale as has already been established. In-phase displacements will result in a purely positive contribution to the atomic displacement correlations which corresponds to a smaller $\beta_{uvw,ij}^{mn}$ relative to the uncorrelated case for all interatomic distances. On the contrary, the antiphase displacement contributions will alternate in sign

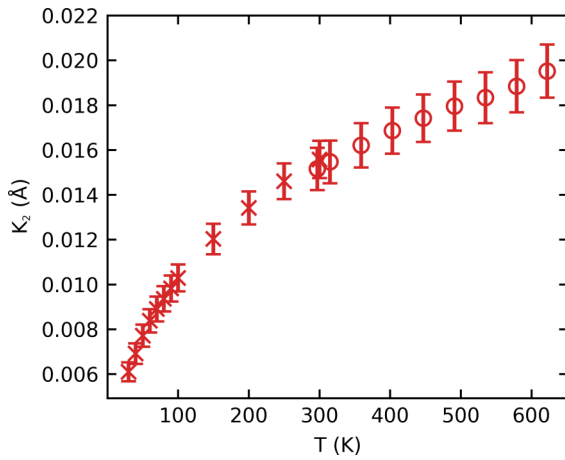


FIG. 6. Fitted values of K_2 as a function of temperature. Error bars represent $\pm\sigma$ estimated from the least-squares fit. x's correspond to data on crystal A while circles correspond to crystal B.

along $\langle 100 \rangle$ corresponding to negative and positive contributions to $\beta_{uvw,ij}^{mn}$. This motivates fitting the root-mean-square deviation of interatomic distances along $\langle 100 \rangle$ with a constant, to account for the long-distance ADP contribution, and two exponentially decaying functions, one of which alternates in sign with every half integer lattice unit step along $\langle 100 \rangle$,

$$\sqrt{\beta_{u00,11}^{mn}} = K_0 - K_1 e^{-\frac{x}{t_1}} - (-1)^{2x} K_2 e^{-\frac{x}{t_2}}.$$

The weight of the latter function, K_2 , is then considered a measure of the antiphase displacement contribution to $\beta_{uvw,ij}^{mn}$ and is as such a measure of the tendency for Pb-Te “dimerization,” i.e., the tendency of forming local, dynamic dipoles. This measure is plotted as a function of temperature in Fig. 6. More information about the fitting procedure can be found in the Supplemental Material [35].

As observed from Fig. 6 the dynamic dipole formation increases with temperature showing a trend similar to what was observed in [27,28]. Thus, although we see a larger relative antiphase contribution to the displacement correlations at low temperatures, the local dipole formation, which depends on the absolute amount of antiphase displacements, increases

with temperature consistent with the observations made by Jensen *et al.* and Božin *et al.* [27,28].

Having now analyzed the PbTe system and its formation of dynamic local dipoles as a function of temperature, it is relevant to consider a related system in order to understand the underlying mechanisms responsible for the soft mode dynamics and local dipole formation. In the following section we analyze the diffuse scattering from KCl as an example of a system with no significant soft-mode contributions to the dynamics, and the differences between KCl and PbTe are then interpreted in terms of differences in bonding.

D. Relation to an archetypical rocksalt system, KCl

In Fig. 7(a) the diffuse scattering from KCl is shown in the $L = 0$ plane of reciprocal space along with the model intensity and residuals from the YELL refinement. Although the diffuse scattering at first glance might look similar to that of PbTe, there are significant differences. While lines running between symmetry-allowed Bragg reflections are still present, see Fig. 7(a), the secondary lines running between the forbidden reflections observed for PbTe are not present for KCl. The shapes of the diffuse scattering features surrounding allowed Bragg reflections shown in Fig. 7(a) are qualitatively very similar to the shapes calculated by Lonsdale [14] using the equations derived by Jahn [50]. This correspondence is particularly relevant as the equations derived by Jahn are based on neglecting the contribution of the optical-phonon modes to TDS, while only including the contributions from acoustic modes. For KCl this is a reasonable approximation, as no soft optical modes are present [34].

The 3D- Δ PDF obtained by Fourier transforming the experimental diffuse scattering is shown in Fig. 7(b) and clearly shows the positive displacement correlations. The refined displacement correlations from YELL shown in Fig. 7(c) also display the expected trend corresponding to no significant antiphase displacement contributions to the dynamics. This further supports the interpretation of the displacement correlations observed for PbTe.

The observed differences between PbTe and KCl can be described in terms of the soft TO phonon mode, but the fundamental difference must be understood in terms of their chemical bonding. In order to understand this, we need to

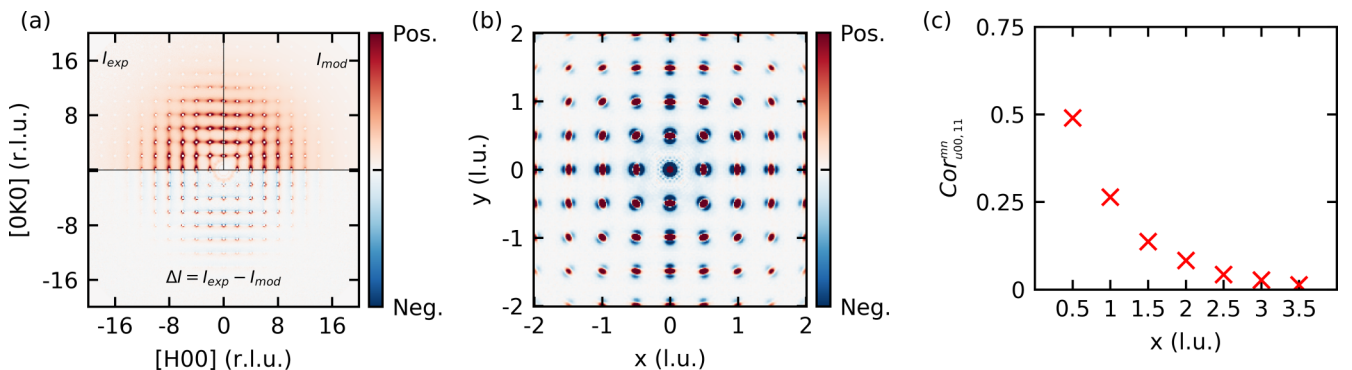


FIG. 7. (a) Experimental and modelled diffuse scattering for KCl in the $L = 0$ plane at 300 K (top left and right quadrants respectively) and the corresponding refinement residuals (bottom half). (b) 3D- Δ PDF obtained by Fourier transforming the diffuse scattering—the negative-positive features clearly show positive displacement correlations. (c) Longitudinal displacement correlations along $\langle 100 \rangle$.

invoke the two concepts of resonant bonding (or metavalent bonding, *vide infra*) and stereochemically active lone pairs, which are highly complementary for understanding the bonding and properties in IV-VI semiconductors. Both concepts have been used in the interpretation of low thermal conductivity in these and related materials [49,51–54].

The bonding and low thermal conductivity in PbTe and related systems has recently been interpreted in the resonant bonding picture by Lee *et al.* [49] originally proposed by Lucovsky and White [55]. For PbTe in the average rock-salt structure, six equivalent unsaturated two-center—one-electron ($2c - 1e$) σ bonds are formed between Pb and Te. Considering the zone-center TO mode, the corresponding atomic displacements break the equivalence of the σ bonds resulting in a redistribution of electron density, which leads to a strong electron-phonon coupling and a large polarizability evidenced by the large transverse Born effective charge in PbTe [56]. The strong electron-phonon coupling promotes long-range interactions, which leads to a softening of the TO mode [49].

Recently, it has been proposed that the resonant bonding in IV-VI semiconductors should be termed metavalent bonding [57,58] as their bonding and response properties are significantly different from materials conventionally associated with the resonant bonding concept (e.g., graphite). Since the resonant bonding of PbTe is related to σ bonding, while the resonant bonding of graphite is related to π bonding and is added on top of the rigid σ bonding of the sp^2 network, it is reasonable that their response properties do not display the same trends, and a different term for the bonding mechanism is needed to clearly distinguish them.

The argument that the long-range interactions originate from resonant or metavalent bonding is based on the observation that the electron density of the p band is strongly perturbed by atomic displacement compared to the s band [49]. However, this interpretation neglects the presence of a small, but nonzero contribution of cation s states at the valence-band maximum (VBM), arising from mixing of the formal cation s lone pair and anion p states resulting in the formation of antibonding states close to the VBM [59]. Upon distortion, the formally empty cation p states are allowed to hybridize with this antibonding state, leading to an orbital stabilization and the expression of an anion-mediated stereochemically active lone pair on the cation [60]. This hybridization does not lead to stabilization in an undistorted structure, and thus displacement along the zone center TO mode is associated with a stabilizing orbital effect. The resulting formation of a short $2c - 2e$ Pb-Te bond and the expression of a stereochemically active lone pair on the opposite side of Pb is clearly evident from the electron localization function calculated by Sangiorgio *et al.* [12].

On the other hand, KCl has no s -like lone pair and rather than unsaturated σ bonds, the bonding is ionic with an almost complete charge transfer from K to Cl. Upon atomic displacement in KCl, no stabilizing lone pair effects are present, and therefore no soft TO mode is observed.

Thus, we argue that the origin of the soft TO phonon mode is strongly related to the ability to express a stereochemically active lone pair upon atomic displacement. The resonant or metavalent bonding model is useful for describing the dif-

ference in ground-state bonding of PbTe and KCl, and the unsaturated σ bonds in PbTe allow for the transition between $2c - 1e$ bonds and $2c - 2e$ bonds upon displacement and the formation of local dipoles through dimerization. Similarly, the arguments based on a strong electron-phonon coupling and large polarizability leading to long-range interactions remain valid. However, it is important to acknowledge that the origin of the large coupling is the stabilizing effect of the dynamic expression of the stereochemically active lone pair.

Indications of local dipole formation have also been observed for the related lead chalcogenides PbS and PbSe [27,29] using one-dimensional PDF techniques. It would be of interest to further characterize these compounds in a manner similar to what has been done for PbTe here. Hereby, the variation of local dipole formation and phonon softening could be related to the identity of the chalcogen atom which could possibly shed more light on the physical significance of the dynamically expressed stereoactive lone pair.

IV. CONCLUSION

The structure of PbTe has been discussed widely in recent years due to the technological relevance of PbTe-based thermoelectric materials. One key point of discussion has been the origin of the low lattice thermal conductivity which has been attributed to the anharmonic soft-mode dynamics of the system. Here, the x-ray single-crystal diffuse scattering at temperatures between 30 and 622 K has been analyzed in detail in order to investigate the temperature dependence of the dynamic local dipole formation believed to result from the soft-mode dynamics.

It is found that the qualitative 3D- Δ PDFs and the steplike trend of extracted atomic displacement correlations along $\langle 100 \rangle$ may be explained by the TO soft-mode dynamics over the full temperature range. The relative contribution of the near zone-center TO modes to displacement correlations increases with decreasing temperature as the softening of the TO branch mitigates the effect of a lower temperature on the phonon population. However, the formation of dynamic dipoles, which depends on the absolute amount of antiphase displacements to the dynamics, is observed to occur upon heating, consistent with previous studies.

Upon comparing PbTe to the KCl system we observe that KCl displays no significant antiphase displacement contributions to the correlations along $\langle 100 \rangle$. This is expected based on chemical bonding considerations. In PbTe, the dynamic expression of the anion mediated lone pair along with the concomitant transition between two-center—one-electron ($2c - 1e$) and $2c - 2e$ bonds gives rise to a softening of the TO branch near the Brillouin-zone center. Contrarily, the lack of an s -like lone pair and metavalent bonding in KCl results in no softening of the TO branch. Thus, the differences in phonon dispersions and the resulting displacement correlations is expected based on the differences in chemical bonding in the two systems.

ACKNOWLEDGMENTS

The authors gratefully acknowledge M. von Zimmermann for sharing his script for converting raw data to reciprocal

space. This work was supported by the Villum Foundation and the Danish Agency for Science, Technology and Innovation (DanScatt). Affiliation with the Aarhus University Center for Integrated Materials Research (iMAT) is gratefully acknowledged. The synchrotron experiments were performed at

Spring-8 BL02B1 with the approval of the Japan Synchrotron Radiation Research Institute (JASRI) as a Partner User (Proposals No. 2017B0078, No. 2018A0078, No. 2018B0078, and No. 2019A0159). Beamline scientist K. Sugimoto is acknowledged for support during synchrotron experiments.

- [1] *Acta Cryst. Sect. A* **48**, 922 (1992).
- [2] A. Simonov, T. De Baerdemaeker, H. L. B. Boström, M. L. Ríos Gómez, H. J. Gray, D. Chernyshov, A. Bosak, H.-B. Bürgi, and A. L. Goodwin, *Nature (London)* **578**, 256 (2020).
- [3] R. Withers, *IUCrJ* **2**, 74 (2015).
- [4] R. L. Withers, E. Urones-Garrote, and L. C. Otero-Diaz, *Philos. Mag.* **87**, 2807 (2007).
- [5] J. Billingham, P. S. Bell, and M. H. Lewis, *Acta Cryst. Sect. A* **28**, 602 (1972).
- [6] M. Sauvage and E. Parthe, *Acta Cryst. Sect. A* **28**, 607 (1972).
- [7] N. Roth and B. B. Iversen, *Acta Cryst. Sect. A* **75**, 465 (2019).
- [8] M. Hostettler, H. Birkedal, and D. Schwarzenbach, *Acta Cryst. Sect. B* **58**, 903 (2002).
- [9] H. Jagodzinski, *Acta Cryst.* **2**, 201 (1949).
- [10] H. Jagodzinski, *Acta Cryst.* **2**, 298 (1949).
- [11] H. Jagodzinski, *Acta Cryst.* **2**, 208 (1949).
- [12] B. Sangiorgio, E. S. Bozin, C. D. Malliakas, M. Fechner, A. Simonov, M. G. Kanatzidis, S. J. L. Billinge, N. A. Spaldin, and T. Weber, *Phys. Rev. Mater.* **2**, 085402 (2018).
- [13] R. Q. Xu and T. C. Chiang, *Z. Kristallogr.* **220**, 1009 (2005).
- [14] K. Lonsdale, *Phys. Soc.* **54**, 314 (1942).
- [15] T. R. Welberry, D. J. Goossens, A. J. Edwards, and W. I. F. David, *Acta Cryst. Sect. A* **57**, 101 (2001).
- [16] T. Weber and A. Simonov, *Z. Kristallogr.* **227**, 238 (2012).
- [17] M. J. Krogstad, S. Rosenkranz, J. M. Wozniak, G. Jennings, J. P. C. Ruff, J. T. Vaughney, and R. Osborn, *Nat. Mater.* **18**, 1384 (2019).
- [18] A. Simonov, T. Weber, and W. Steurer, *J. Appl. Cryst.* **47**, 2011 (2014).
- [19] G. J. Snyder and E. S. Toberer, *Nat. Mater.* **7**, 105 (2008).
- [20] T. Egami and S. J. L. Billinge, *Underneath the Bragg Peaks: Structural Analysis of Complex Materials*, Pergamon Materials Series No. 7 (Pergamon Press, Kington, Oxford, UK, 2003).
- [21] G. A. Akhmedova and D. S. Abdinov, *Inorg. Mater.* **45**, 854 (2009).
- [22] Y. Z. Pei, X. Y. Shi, A. LaLonde, H. Wang, L. D. Chen, and G. J. Snyder, *Nature* **473**, 66 (2011).
- [23] C. W. Li, O. Hellman, J. Ma, A. F. May, H. B. Cao, X. Chen, A. D. Christianson, G. Ehlers, D. J. Singh, B. C. Sales, and O. Delaire, *Phys. Rev. Lett.* **112**, 175501 (2014).
- [24] O. Delaire, J. Ma, K. Marty, A. F. May, M. A. McGuire, M.-H. Du, D. J. Singh, A. Podlesnyak, G. Ehlers, M. D. Lumsden, and B. C. Sales, *Nat. Mater.* **10**, 614 (2011).
- [25] T. Shiga, J. Shiomi, J. Ma, O. Delaire, T. Radzyski, A. Lusakowski, K. Esfarjani, and G. Chen, *Phys. Rev. B* **85**, 155203 (2012).
- [26] R. Hanus, M. T. Agne, A. J. E. Rettie, Z. Chen, G. Tan, D. Y. Chung, M. G. Kanatzidis, Y. Pei, P. W. Voorhees, and G. J. Snyder, *Adv. Mater.* **31**, 1900108 (2019).
- [27] E. S. Bozin, C. D. Malliakas, P. Souvatzis, T. Proffen, N. A. Spaldin, M. G. Kanatzidis, and S. J. L. Billinge, *Science* **330**, 1660 (2010).
- [28] K. M. O. Jensen, E. S. Bozin, C. D. Malliakas, M. B. Stone, M. D. Lumsden, M. G. Kanatzidis, S. M. Shapiro, and S. J. L. Billinge, *Phys. Rev. B* **86**, 085313 (2012).
- [29] R. Z. Yu, E. S. Bozin, M. Abeykoon, B. Sangiorgio, N. A. Spaldin, C. D. Malliakas, M. G. Kanatzidis, and S. J. L. Billinge, *Phys. Rev. B* **98**, 144108 (2018).
- [30] S. Christensen, N. Bindzus, M. Sist, M. Takata, and B. B. Iversen, *Phys. Chem. Chem. Phys.* **18**, 15874 (2016).
- [31] S. Christensen, N. Bindzus, M. Christensen, and B. B. Iversen, *Acta Cryst. Sect. A* **71**, 9 (2015).
- [32] C. M. Zeuthen, P. S. Thorup, N. Roth, and B. B. Iversen, *J. Am. Chem. Soc.* **141**, 8146 (2019).
- [33] S. Kastbjerg, N. Bindzus, M. Sondergaard, S. Johnsen, N. Lock, M. Christensen, M. Takata, M. A. Spackman, and B. B. Iversen, *Adv. Func. Mater.* **23**, 5477 (2013).
- [34] J. R. D. Copley, R. W. Macpherson, and T. Timusk, *Phys. Rev.* **182**, 965 (1969).
- [35] See Supplemental Material at <http://link.aps.org/supplemental/10.1103/PhysRevB.102.024112> for details on average structure data reduction and solution, reciprocal space reconstruction and treatment of Bragg peaks, treatment of background in diffuse scattering data, modeling of diffuse scattering, R values from diffuse scattering modeling, fitting procedure of root-mean-square deviations of interatomic distances, and additional examples of diffuse scattering and corresponding 3D- Δ PDFs.
- [36] R. H. Blessing, *Acta Cryst. Sect. A* **51**, 33 (1995).
- [37] R. H. Blessing, *J. Appl. Cryst.* **30**, 421 (1997).
- [38] G. M. Sheldrick, *Acta Cryst. Sect. C* **71**, 3 (2015).
- [39] V. Petricek, M. Dusek, and L. Palatinus, *Z. Kristallogr.* **229**, 345 (2014).
- [40] M. Adam, E. Hovestreydt, M. Ruf, and J. Kaercher, *Acta Cryst. Sect. A* **71**, S194 (2015).
- [41] L. Krause, R. Herbst-Irmer, G. M. Sheldrick, and D. Stalke, *J. Appl. Cryst.* **48**, 3 (2015).
- [42] L. Krause, K. Tolborg, T. B. E. Gronbech, K. Sugimoto, B. B. Iversen, and J. Overgaard, *J. Appl. Cryst.* **53**, 635 (2020).
- [43] B. T. M. Willis and A. W. Pryor, *Thermal Vibrations in Crystallography* (Cambridge University Press, London, 1975).
- [44] A. Bentien, E. Nishibori, S. Paschen, and B. B. Iversen, *Phys. Rev. B* **71**, 144107 (2005).
- [45] M. V. Zimmerman (unpublished).
- [46] A. Simonov, T. Weber, and W. Steurer, *J. Appl. Cryst.* **47**, 1146 (2014).
- [47] M. Kobas, T. Weber, and W. Steurer, *Phys. Rev. B* **71**, 224205 (2005).
- [48] M. J. Cooper and K. D. Rouse, *Acta Cryst. Sect. A* **29**, 514 (1973).
- [49] S. Lee, K. Esfarjani, T. F. Luo, J. W. Zhou, Z. T. Tian, and G. Chen, *Nat. Commun.* **5**, 3525 (2014).
- [50] H. A. Jahn, *Proc. R. Soc. London, Ser. A* **180**, 0476 (1942).
- [51] E. J. Skoug and D. T. Morelli, *Phys. Rev. Lett.* **107**, 235901 (2011).

- [52] M. D. Nielsen, V. Ozolins, and J. P. Heremans, *Energ. Environ. Sci.* **6**, 570 (2013).
- [53] Y. Yu, M. Cagnoni, O. Cojocaru-Mirédin, and M. Wuttig, *Adv. Funct. Mater.* **30**, 1904862 (2020).
- [54] K. Tolborg, C. Gatti, and B. B. Iversen, *IUCrJ* **7**, 480 (2020).
- [55] G. Lucovsky and R. M. White, *Phys. Rev. B* **8**, 660 (1973).
- [56] P. B. Littlewood and V. Heine, *J. Phys. C* **12**, 4431 (1979).
- [57] M. Wuttig, V. L. Deringer, X. Gonze, C. Bichara, and J. Y. Raty, *Adv. Mater.* **30**, 1803777 (2018).
- [58] J. Y. Raty, M. Schumacher, P. Golub, V. L. Deringer, C. Gatti, and M. Wuttig, *Adv. Mater.* **31**, 1806280 (2019).
- [59] U. V. Waghmare, N. A. Spaldin, H. C. Kandpal, and R. Seshadri, *Phys. Rev. B* **67**, 125111 (2003).
- [60] A. Walsh, D. J. Payne, R. G. Egdell, and G. W. Watson, *Chem. Soc. Rev.* **40**, 4455 (2011).